Research Square

Preprints are preliminary reports that have not undergone peer review.
They should not be considered conclusive, used to inform clinical practice,
or referenced by the media as validated information.

Reduced Persistence of Cortical States in Benign Paroxysmal Positional Vertigo: A Hidden Markov Model Analysis of Resting-State Functional Magnetic Resonance Imaging

Yutao Wang[1]
First Affiliated Hospital of Xi'an Jiaotong University
Ke Yang[1]
First Affiliated Hospital of Xi'an Jiaotong University
Yi Zhang[1]
First Affiliated Hospital of Xi'an Jiaotong University
Yuxin Fan[1]
First Affiliated Hospital of Xi'an Jiaotong University
Juanli Xing[2]
First Affiliated Hospital of Xi'an Jiaotong University
Yanning Yuan[2]
First Affiliated Hospital of Xi'an Jiaotong University
Yuan Wang[1]
wangyuan8003@126.com
First Affiliated Hospital of Xi'an Jiaotong University

Research Article

Keywords: Benign paroxysmal positional vertigo, Functional magnetic resonance imaging, Hidden Markov model, Brain mapping, Vestibular system

Posted Date: November 1st, 2026

DOI: https://doi.org/10.21203/rs.3.rs-10717212/v1

License: This work is licensed under a Creative Commons Attribution 4.0 International License.
Read Full License

Additional Declarations: No competing interests reported.

Abstract

To determine whether hidden Markov model (HMM) analysis of resting-state functional MRI (fMRI) can identify altered temporal persistence of recurring cortical states in patients with benign paroxysmal positional vertigo (BPPV). This cross-sectional study included 70 patients with BPPV and 46 healthy controls. Time series from 100 cortical parcels were analyzed using a five-state Gaussian HMM specified a priori. Switching rate was the primary outcome, and mean empirical self-transition probability was a supporting measure. Group comparisons were adjusted for age, sex, years of education, and mean framewise displacement, with false-discovery-rate correction. Sensitivity analyses evaluated head motion, model orders K = 2–15, and omission of global signal regression. Switching rate was higher in patients with BPPV than in controls (0.417 ± 0.030 vs 0.370 ± 0.035; adjusted β = 0.047; 95% confidence interval, 0.035–0.060; q = 3.61 × 10 − 11). Mean empirical self-transition probability was lower in the patient group (0.573 ± 0.027 vs 0.623 ± 0.035; adjusted β = −0.049; 95% confidence interval, − 0.061 to − 0.037; q = 8.04 × 10 − 12). Patients with BPPV also showed higher fractional occupancy of State 2 and lower fractional occupancy of State 3. Both global effects remained directionally consistent across sensitivity analyses. BPPV was associated with reduced persistence of recurring cortical states on resting-state fMRI. Temporally resolved HMM analysis may complement conventional time-averaged functional imaging measures.

Introduction

Benign paroxysmal positional vertigo (BPPV) is a common peripheral vestibular disorder characterized by brief episodes of positionally triggered vertigo and nystagmus (von Brevern et al. 2015; Bhattacharyya et al. 2017). Vestibular perception and postural control require continuous integration of vestibular, visual, somatosensory, and spatial information (Wu et al. 2024; Xing et al. 2024). During an episode of BPPV, recurrent positional symptoms provide a clinically defined window in which to examine how ongoing peripheral vestibular disturbance is associated with the temporal organization of cortical activity.

Previous neuroimaging studies of BPPV and residual dizziness have reported alterations in regional activity (Fu et al. 2022; Lin et al. 2023) and functional connectivity (Chen et al. 2024d; Chen et al. 2024c), including changes involving multisensory vestibular, visual, default mode, and spatial-orientation networks (Chen et al. 2024b; Yang et al. 2026). Related vestibular imaging studies have also implicated distributed cortical (Xing et al. 2024) and subcortical systems in persistent dizziness and compensation (Teh et al. 2022; Chen et al. 2024a). However, these studies primarily quantified time-averaged regional activity or functional connectivity, and the corresponding measures cannot determine whether group differences reflect altered occupancy of recurring cortical configurations or more frequent reconfiguration over time.

Hidden Markov models identify recurring multivariate cortical states (Ezaki et al. 2021; Moretto et al. 2022) and estimate the temporal sequence in which they occur (Vidaurre et al. 2025). Switching rate

quantifies how often the decoded sequence changes state, whereas empirical self-transition probability quantifies the conditional probability that the decoded sequence remains in the same state at the next time point. These measures provide temporal information that is not captured by time-averaged analyses (Chen et al. 2022; Long et al. 2023). If BPPV is associated with less stable multisensory cortical organization, patients would be expected to switch more frequently between recurring distributed states.

The objective of this study was to determine whether HMM analysis of resting-state fMRI could identify altered temporal persistence of recurring cortical states in BPPV. We hypothesized that BPPV patients would show reduced persistence, reflected primarily by a higher switching rate and supported by a lower mean empirical self-transition probability. A five-state model was specified a priori. Mean dwell time and mean number of visits per state were retained as descriptive summaries of the same decoded run structure; fractional occupancy and state-specific empirical transition probabilities were secondary outcomes. Sensitivity analyses evaluated head motion, model order, and global signal regression, and clinical associations were exploratory.

Materials and Methods

Study Design and Participants

This observational cross-sectional study initially included 129 participants: 79 patients with BPPV and 50 healthy controls. A prespecified subject-level motion criterion excluded participants if more than 20% of the 180 analyzed volumes had framewise displacement > 0.5 mm. This criterion excluded 12 participants: nine patients and three healthy controls. One healthy control was excluded because at least one extracted cortical parcel time series contained only zeros or had zero variance. The final sample comprised 70 patients and 46 healthy controls. BPPV was diagnosed according to the diagnostic criteria of the Bárány Society (von Brevern et al. 2015), based on positionally triggered vertigo and characteristic positional nystagmus elicited by the Dix–Hallpike and/or supine roll test. All patients had undergone canalith repositioning before MRI.

Exclusion criteria were other types of vestibular disorders, major neurological or psychiatric disorders, clinically relevant structural brain abnormalities, major head trauma, substance misuse, or MRI contraindications. Healthy controls had no history of recurrent vertigo or diagnosed vestibular disorder. All eligible participants with complete quality-controlled data were included. Some participants had been included in previous reports from the same imaging cohort that examined static functional connectivity or gray-matter structure (Yang et al. 2026; Liu et al. 2025). The present analysis addresses a separate research question and reports previously unpublished HMM-derived outcomes.

Clinical Assessment

Clinical assessments included the Dizziness Handicap Inventory, Activities-specific Balance Confidence Scale, vertigo visual analog scale, and postural visual analog scale (Lee et al. 2021). All of the measures were available for all 70 patients. For association analyses, the Activities-specific Balance Confidence score was reverse-coded as 100 minus the original score so that higher values indicated greater impairment. Continuous clinical measures and HMM-derived summaries were standardized within the patient group. Clinical measures were not used for HMM fitting, state selection, or primary group comparisons. Sex was obtained from the clinical records and included as a covariate in all primary group-level models.

This study was performed in line with the principles of the Declaration of Helsinki. Approval was granted by the Ethics Committee of the First Affiliated Hospital of Xi'an Jiaotong University on March 2, 2023 (Approval No. XJTU1AF2023LSK-566). Written informed consent was obtained from all participants.

MRI Data Acquisition

Imaging was acquired on a 3.0-T Discovery MR750w system (GE Healthcare, Milwaukee, WI, USA) using a 64-channel head coil. During resting-state functional MRI, participants were instructed to keep their eyes closed and remain still. Resting-state blood-oxygen-level-dependent data were acquired using gradient-echo echo-planar imaging (repetition time = 2500 ms, echo time = 30 ms, flip angle = 90°, field of view = 22.4 cm, matrix = 64 × 64, slice thickness = 3.5 mm, no gap). A total of 188 volumes were acquired. The first eight volumes were discarded to allow signal equilibration, leaving 180 volumes for analysis. High-resolution T1-weighted anatomical images were acquired in the axial plane using a three-dimensional BRAVO sequence (inversion time = 600 ms, flip angle = 8°, field of view = 256 mm, acquisition matrix = 256 × 256, slice thickness = 1.0 mm, 170 slices, and a nominal voxel size of 1.0 × 1.0 × 1.0 mm^3).

Image Preprocessing and Time-Series Extraction

Structural and functional images were processed using fMRIPrep version 25.2.3 (Esteban et al. 2019). Preprocessing included intensity-nonuniformity correction, brain extraction, tissue segmentation, spatial normalization, blood-oxygen-level-dependent reference generation, rigid-body motion estimation, registration of the functional series to the T1-weighted image, and resampling to standard space. Post-fMRIPrep denoising and cortical time-series extraction were performed using Nilearn version 0.13.1 in Python 3.10 (Abraham et al. 2014). Regional signals were extracted from 100 cortical parcels in the Schaefer 2018 atlas (Schaefer et al. 2018). Within each participant, the extracted parcel time series were detrended, band-pass filtered at 0.01–0.10 Hz, nuisance-regressed, and standardized separately for each parcel within a single Nilearn cleaning operation. The nuisance model included 24 motion parameters, mean white-matter and cerebrospinal-fluid signals, the global signal, and separate single-volume regressors for volumes with framewise displacement > 0.2 mm or standardized DVARS > 3 (Ciric et al.

2017; Parkes et al. 2018). Spike-flagged volumes were retained in the time series and modeled using volume-specific regressors rather than removed before HMM fitting.

Mean framewise displacement was included as a participant-level covariate. Maximum framewise displacement and the proportion of volumes with framewise displacement > 0.5 mm were retained for descriptive and sensitivity analyses. Both patient and control groups contributed 180 time points per participant and were represented using the same cortical parcellation.

Hidden Markov Model Analysis

The cerebral cortex was represented by 100 parcels from the Schaefer 2018 atlas, with network labels assigned according to the Yeo seven-network parcellation (Schaefer et al. 2018; Yeo et al. 2011). Standardized parcel time series were concatenated across participants, and participant-specific sequence lengths were supplied to preserve sequence boundaries during model fitting and decoding. The five-state model order was specified a priori. A Gaussian HMM with diagonal covariance was fitted using hmmlearn version 0.3.2 in Python. The model was fitted 50 times from random initializations, and the converged solution with the highest final log likelihood was selected for participant-level Viterbi decoding. Group labels were not used during model fitting, solution selection, or decoding.

Each participant contributed a decoded sequence of 180 time points. Viterbi decoding assigned the most likely state label to each time point. The fitted model therefore defined a common state space before participant-level summaries were compared between groups. The analysis workflow is summarized in Fig. 1.

HMM-Derived Metrics

Let S denote the number of changes between adjacent state labels in a decoded sequence of length T = 180. Switching rate was calculated as $S/(T - 1) = S/179$ and served as the primary measure of sequence fragmentation.

The S state changes define S + 1 contiguous state runs. Mean number of visits per state was calculated as $(S + 1)/5$, and mean dwell time was calculated as $T/(S + 1)$ time points. At fixed T and K, switching rate, mean number of visits per state, and mean dwell time are deterministic functions of the same decoded run structure. Switching rate was therefore treated as the primary inferential outcome, whereas the other two measures were retained as descriptive summaries. Fractional occupancy was defined as the proportion of time points assigned to each state.

For each participant and current state i, the empirical decoded-sequence transition probability from state i to state j was calculated as the number of observed i→j transitions divided by the total number of transitions originating from state i. Mean empirical self-transition probability was calculated as the unweighted mean of the five diagonal i→i probabilities. All participants had at least one valid outgoing transition from each state, allowing all five diagonal probabilities to contribute to the participant-level

mean. Because this measure averages state-specific conditional probabilities, it is not determined solely by the total number of state changes and was treated as a supporting measure of state persistence. State maps represent means of standardized parcel signals within the fitted model and should not be interpreted as absolute neural activation.

Sensitivity Analyses

Because K = 5 was specified a priori, analyses across K = 2–15 were treated as sensitivity analyses rather than as a model-selection procedure. Motion sensitivity was examined using three complementary approaches. First, maximum framewise displacement and the proportion of volumes with framewise displacement > 0.5 mm were added to the primary covariate set. Second, analyses were repeated after restricting the sample to participants with maximum framewise displacement ≤ 2.0 mm. Third, a censor-aware analysis was performed on the decoded sequences from the primary HMM without refitting the model. Volumes with framewise displacement > 0.2 mm or standardized DVARS > 3 were treated as sequence breaks, and adjacent pairs containing a flagged volume were excluded. Switching rate and mean empirical self-transition probability were recomputed from the remaining valid adjacent pairs and tested using the primary covariate set. Within each group, Spearman correlations assessed the associations of both censor-aware measures with mean framewise displacement, maximum framewise displacement, and the proportion of volumes with framewise displacement > 0.5 mm.

Model-order sensitivity analyses evaluated global temporal measures across K = 2–15. For visualization and comparison across model orders, each K-specific measure was z-standardized across all participants before fitting the same covariate-adjusted group model. The plotted coefficient represents the adjusted BPPV-minus-control difference in standard-deviation units, with corresponding 95% confidence intervals. For the analysis without global signal regression, all preprocessing steps were identical except that global-signal terms were omitted from the nuisance model. A separate HMM was fitted to assess the direction of the global temporal effects; state-specific correspondence between preprocessing pipelines was not assumed.

Clinical associations were evaluated within the BPPV group. Each of the four vertigo measures was tested against each of the four global HMM summaries, yielding 16 covariate-adjusted models. Models included age, sex, years of education, and mean framewise displacement. Benjamini–Hochberg false-discovery-rate (FDR) correction was applied across the 16 tests. These cross-sectional analyses were exploratory and were not designed to assess individual-level diagnostic or prognostic performance.

Statistical Analysis

Participant-level ordinary least-squares regression models included group (BPPV = 1, healthy control = 0), age, sex (male = 1, female = 0), years of education, and mean framewise displacement. Group effects are reported as adjusted BPPV-minus-control coefficients with 95% confidence intervals, t statistics, and

two-sided P values. FDR–adjusted q values < 0.05 were considered statistically significant (Benjamini et al. 1995). Switching rate was the primary inferential outcome, and mean empirical self-transition probability was a supporting outcome. Raw and FDR-adjusted P values are reported for all four global temporal measures, but mean dwell time and mean number of visits per state were not interpreted as independent evidence because they are deterministic transformations of the same decoded run structure. Separate correction families comprised the five fractional-occupancy tests, the 25 state-specific empirical transition tests, and the 16 clinical association tests.

Model diagnostics assessed residual normality, heteroscedasticity, and influential observations. Complete-case analysis was used; all covariates were complete in the final sample, and all four vertigo measures were available for the 70 patients. Table 1 comparisons used Welch's t test for age, education, and mean framewise displacement; the Mann–Whitney U test for maximum framewise displacement and the proportion of volumes with framewise displacement > 0.5 mm; and Pearson's chi-square test for sex. All tests were two-sided.

Table 1
Demographic, clinical, and imaging-quality characteristics of the study sample

Variable	BPPV (n = 70)	HC (n = 46)	Test statistic	P value
A. Demographic and imaging quality characteristics				
Age, years	45.01 ± 8.50	44.48 ± 7.46	t = − 0.36	0.721
Sex, male/female, n	14/56	13/33	$\chi^2(1) = 1.06$	0.303
Education, years	13.54 ± 4.14	12.98 ± 3.35	t = − 0.81	0.421
Mean FD, mm	0.107 ± 0.036	0.115 ± 0.041	t = 1.02	0.311
Maximum FD, mm	0.479 [0.372 to 0.781]	1.348 [1.178 to 1.507]	U = 2830	5.88×10^{-12}
Volumes with FD > 0.5 mm, proportion	0.000 [0.000 to 0.011]	0.006 [0.006 to 0.022]	U = 2294	7.28×10^{-5}
B. Clinical characteristics in patients with BPPV				
DHI	38.00 [16.50 to 52.00]	—	—	—
ABC	89.38 [69.62 to 96.88]	—	—	—
VVAS	4.00 [3.00 to 6.00]	—	—	—
PVAS	2.00 [0.00 to 4.00]	—	—	—

Values are presented as mean ± standard deviation or median [25th to 75th percentile], as appropriate. All clinical measures were available for all 70 patients. BPPV, benign paroxysmal positional vertigo; HC, healthy control; FD, framewise displacement; DHI, Dizziness Handicap Inventory; ABC, Activities-specific Balance Confidence Scale; VVAS, vertigo visual analog scale; PVAS, postural visual analog scale. All tests were two-sided.

Results

Participant Characteristics

The final sample comprised 70 patients with BPPV and 46 healthy controls. The two groups did not differ in age, sex, years of education, or mean framewise displacement (all P > 0.30). Maximum framewise displacement and the proportion of volumes with framewise displacement > 0.5 mm were higher in healthy controls, motivating the motion sensitivity analyses. All four vertigo measures were available in the BPPV group (Table 1).

Cortical Expression States

The primary model identified five recurring cortical expression states (Fig. 2). State 2 showed relatively greater expression in the default mode network, whereas State 3 showed only small deviations from zero across the seven networks. These patterns represent state-specific means of standardized parcel signals within the fitted HMM rather than absolute neural activation.

Global Temporal Dynamics

Switching rate was higher in patients with BPPV (0.417 ± 0.030) than in healthy controls (0.370 ± 0.035; adjusted β = 0.047, 95% confidence interval 0.035 to 0.060; t(110) = 7.41; P = 2.71 × 10 − 11; q = 3.61 × 10 − 11; Fig. 3 and Table 2). Mean empirical self-transition probability was lower in patients with BPPV (0.573 ± 0.027) than in healthy controls (0.623 ± 0.035; adjusted β = −0.049, 95% confidence interval − 0.061 to − 0.037; t(110) = − 7.93; P = 2.01 × 10 − 12; q = 8.04 × 10 − 12). Mean dwell time was shorter in BPPV patients (adjusted β = −0.305, 95% confidence interval − 0.387 to − 0.222; t(110) = − 7.33; P = 4.05 × 10 − 11; q = 4.05 × 10 − 11), and the mean number of visits per state was higher (adjusted β = 1.687, 95% confidence interval 1.236 to 2.138; t(110) = 7.41; P = 2.71 × 10 − 11; q = 3.61 × 10 − 11) than controls. Because mean dwell time and mean number of visits per state are deterministic functions of the same decoded run structure as switching rate, they were treated as descriptive summaries rather than independent findings.

Table 2
HMM-derived global temporal measures in the primary five-state model

Outcome	BPPV (n = 70)	HC (n = 46)	Adjusted β (95% CI)	t(df)	P value	FDR q value	Cohen's d
Switching rate	0.417 ± 0.030	0.370 ± 0.035	0.047 (0.035 to 0.060)	7.41 (110)	2.71×10^{-11}	3.61×10^{-11}	1.47
Mean dwell time, time points	2.391 ± 0.172	2.700 ± 0.255	−0.305 (− 0.387 to − 0.222)	−7.33 (110)	4.05×10^{-11}	4.05×10^{-11}	−1.48
Mean number of visits per state	15.134 ± 1.072	13.448 ± 1.252	1.687 (1.236 to 2.138)	7.41 (110)	2.71×10^{-11}	3.61×10^{-11}	1.47
Mean empirical self-transition probability	0.573 ± 0.027	0.623 ± 0.035	−0.049 (− 0.061 to − 0.037)	−7.93 (110)	2.01×10^{-12}	8.04×10^{-12}	−1.62

Adjusted β represents the BPPV-minus-HC coefficient from models including age, sex, years of education, and mean framewise displacement. Cohen's d represents the unadjusted standardized mean difference. Switching rate was the primary outcome, and mean empirical self-transition probability was a supporting outcome. Mean dwell time and mean number of visits per state are deterministic functions of the same decoded run structure as switching rate and were not interpreted as independent evidence. BPPV, benign paroxysmal positional vertigo; CI, confidence interval; FD, framewise displacement; HC, healthy control; HMM, hidden Markov model.

Fractional Occupancy and Empirical Transition Probabilities

Fractional occupancy was higher in BPPV patients for State 2 (adjusted β = 0.019, 95% confidence interval 0.004 to 0.035; t(110) = 2.47; P = 0.015; q = 0.037) and lower for State 3 (adjusted β = −0.032, 95% confidence interval − 0.046 to − 0.017; t(110) = − 4.25; P < 0.001; q < 0.001). State 5 showed nominally higher fractional occupancy in patient group (adjusted β = 0.017, 95% confidence interval 0.001 to 0.033; P = 0.039), but the difference did not survive FDR correction (q = 0.066). Fractional occupancy did not differ significantly between the two groups for State 1 or State 4 (q = 0.556 and q = 0.840, respectively).

Six of the 25 empirical transition probabilities survived FDR correction. Empirical self-transition probabilities were lower in BPPV patients for State 1→1 (adjusted β = −0.050; q = 0.017), State 3→3 (adjusted β = −0.091; q < 0.001), and State 4→4 (adjusted β = −0.053; q = 0.005). Between-state empirical transition probabilities were higher for State 3→2 (adjusted β = 0.034; q = 0.005), State 3→4 (adjusted β = 0.029; q = 0.017), and State 5→3 (adjusted β = 0.028; q = 0.029). The complete transition matrix, including adjusted group effects for all 25 empirical transition probabilities, is provided in Online Resource 1, Table S1. Because probabilities within each row sum to one, each transition should be interpreted relative to the other transitions originating from the same state.

These secondary findings indicate a redistribution of empirical transition probabilities within the fitted state space. Figure 4 displays the group-mean matrices, their difference, and the adjusted coefficients for the six transitions that survived false-discovery-rate correction.

Robustness Analyses

Switching rate remained higher in BPPV patients after additional adjustment for maximum framewise displacement and the proportion of high-motion volumes (adjusted β = 0.033, 95% confidence interval 0.015 to 0.050; P < 0.001) and after restriction to participants with maximum framewise displacement ≤ 2.0 mm (adjusted β = 0.046, 95% confidence interval 0.033 to 0.059; P < 0.001). The restricted sample included 43 healthy controls and all 70 BPPV patients. Detailed results from the extended motion-adjusted models and the maximum-FD-restricted sample are provided in Online Resource 1, Table S2. In the censor-aware analysis of decoded sequences from all 116 participants, switching rate remained higher in the patient group (adjusted β = 0.0427, 95% confidence interval 0.0292 to 0.0561; t(110) = 6.30; P = 6.39 × 10 − 9), and mean empirical self-transition probability remained lower (adjusted β = −0.0479, 95% confidence interval − 0.0614 to − 0.0345; t(110) = − 7.05; P = 1.68 × 10 − 10). Within either group, neither censor-aware measure was significantly associated with mean framewise displacement, maximum framewise displacement, or the proportion of high-motion volumes after FDR correction (Online Resource 1, Table S3).

The direction of both global effects was consistent across model orders K = 2–15 and in the analysis without global signal regression: switching rate was higher and mean empirical self-transition probability was lower in BPPV patients than in healthy controls. Model-order results are shown in Fig. 5, and results of the analysis without global signal regression are provided in Online Resource 1, Table S4.

Exploratory Clinical Associations

None of the 16 adjusted associations between the four global HMM summaries and the Dizziness Handicap Inventory, reverse-coded Activities-specific Balance Confidence score, vertigo visual analog scale, or postural visual analog scale survived false-discovery-rate correction (Online Resource 1, Table S5).

Discussion

In this cross-sectional study, patients with BPPV showed more frequent state switching and lower mean empirical self-transition probability than healthy controls, indicating reduced persistence of recurring cortical states. The direction of both effects was consistent across motion-control analyses, model orders K = 2–15, and omission of global signal regression. These results extend prior BPPV imaging studies by characterizing the temporal organization of whole-cortex fMRI signals rather than only their time-averaged regional or connectivity properties.

Vestibular perception and postural control depend on continuous integration of vestibular, visual, somatosensory, and spatial signals (Wu et al. 2024; Xing et al. 2024). During an episode of BPPV, abnormal position-dependent vestibular input may require repeated reweighting across these distributed cortical systems. The observed increase in switching frequency may therefore reflect less stable maintenance of a given multisensory cortical configuration. This interpretation remains provisional because the present data cannot determine whether the altered dynamics represent a direct effect of peripheral vestibular input, a compensatory response, or a nonspecific correlate of clinical symptoms.

Previous functional MRI studies of BPPV and post-repositioning residual dizziness have reported abnormalities involving the precuneus (Fu et al. 2022; Lin et al. 2023), parietal operculum (Chen et al. 2024c), hippocampus (Chen et al. 2024d), default mode network (Chen et al. 2024b), and visual–vestibular connectivity (Wu et al. 2024; Yang et al. 2026). Those studies primarily characterized regional activity or static functional connectivity. The present HMM analysis addresses a complementary question by showing that recurring cortical configurations were less persistent over time in BPPV.

State-specific findings provided secondary detail on the global persistence effect. The BPPV patients showed higher fractional occupancy of State 2, lower fractional occupancy of State 3, lower empirical self-transition probabilities for States 1, 3, and 4, and higher between-state empirical transition probabilities for State 3→2, State 3→4, and State 5→3. Because fractional occupancies and transition probabilities are compositional within the fitted model, these results indicate redistribution within the state space rather than independent effects. State 2 showed relatively greater default mode expression,

but state labels and expression patterns are specific to the fitted HMM (Ezaki et al. 2021; Moretto et al. 2022) and should not be mapped directly onto states obtained from separately fitted models (Vidaurre et al. 2025).

The principal group differences remained consistent after additional adjustment for motion, sample restriction, censor-aware recalculation, model-order variation, and omission of global signal regression. None of the exploratory associations with symptom scales survived FDR correction. Accordingly, the HMM-derived measures should be interpreted as group-level imaging features rather than individual-level diagnostic, prognostic, or symptom markers. Longitudinal studies and validation in independent cohorts are required before the clinical utility of these measures can be assessed.

This study has several limitations. First, its cross-sectional design precludes assessment of within-patient changes after symptom resolution or successful treatment. Second, all patients had undergone canalith repositioning before MRI; therefore, the present design cannot distinguish disease-related alterations from potential responses to the maneuver or other sources of clinical heterogeneity. Third, motion distributions differed between patient and control groups, and residual motion effects remain possible despite multiple sensitivity analyses.

Conclusions

The patients with BPPV showed reduced persistence of recurring cortical states on resting-state fMRI, characterized by more frequent state switching and lower mean empirical self-transition probability. Temporally resolved HMM analysis may complement conventional time-averaged functional imaging measures. Longitudinal studies and validation in independent cohorts are needed to establish reproducibility and clinical relevance.

Declarations

Funding

This work was supported by the National Natural Science Foundation of China [grant number 82171909]; the National Key Research and Development Program of China [grant number 2023YFC2508002]; the Key Research and Development Program of Shaanxi [grant numbers 2025SF-YBXM-328 and 2024SF-YBXM-352]; and the Clinical Research Award of the First Affiliated Hospital of Xi'an Jiaotong University [grant number XJTU1AF-CRF-2023-030]. The funding sources had no role in the study design; data collection, analysis, or interpretation; preparation of the manuscript; or the decision to submit the manuscript for publication.

Competing interests

The authors declare that they have no known competing financial interests or personal relationships that could have appeared to influence the work reported in this paper.

Ethics approval

This study was performed in line with the principles of the Declaration of Helsinki. Approval was granted by the Ethics Committee of the First Affiliated Hospital of Xi'an Jiaotong University on March 2, 2023 (Approval No. XJTU1AF2023LSK-566). Written informed consent was obtained from all participants.

Consent to participate

Written informed consent was obtained from all participants.

Data availability

Individual-level clinical and MRI data are not publicly available because participant consent and institutional ethics approval do not permit unrestricted sharing of potentially sensitive data. De-identified derived data that support the findings may be available from the corresponding author upon reasonable request, subject to institutional approval and execution of an appropriate data-use agreement.

Author contributions

Yutao Wang: Conceptualization, Formal analysis, Writing – original draft. Ke Yang: Investigation, Data curation, Writing – review and editing. Yi Zhang: Investigation, Validation, Writing – review and editing. Yuxin Fan: Data curation, Project administration, Writing – review and editing. Juanli Xing: Methodology, Resources, Writing – review and editing. Yanning Yun: Investigation, Resources, Writing – review and editing. Yuan Wang: Supervision, Funding acquisition, Writing – review and editing.

References

1. Abraham A, Pedregosa F, Eickenberg M et al (2014) Machine learning for neuroimaging with scikit-learn. Front Neuroinform 8. https://doi.org/10.3389/fninf.2014.00014
2. Benjamini Y, Hochberg Y (1995) Controlling the false discovery rate: a practical and powerful approach to multiple testing. J R Stat Soc Ser B Stat Methodol 57(1):289–300. https://doi.org/10.1111/j.2517-6161.1995.tb02031.x
3. Bhattacharyya N, Gubbels SP, Schwartz SR et al (2017) Clinical practice guideline: benign paroxysmal positional vertigo (update). Otolaryngol Head Neck Surg 156. https://doi.org/10.1177/0194599816689667

4. Chen K, Li C, Sun W et al (2022) Hidden Markov modeling reveals prolonged baseline state and shortened antagonistic state across the adult lifespan. Cereb Cortex 32(2):439–453. https://doi.org/10.1093/cercor/bhab220
5. Chen Z, Cai Y, Liu Y et al (2024a) Altered thalamus functional connectivity in patients with acute unilateral vestibulopathy: a resting-state fMRI study. Front Neurosci 18:1388213. https://doi.org/10.3389/fnins.2024.1388213
6. Chen Z, Cai Y, Xiao L et al (2024b) Increased functional connectivity between default mode network and visual network potentially correlates with duration of residual dizziness in patients with benign paroxysmal positional vertigo. Front Neurol 15:1363869. https://doi.org/10.3389/fneur.2024.1363869
7. Chen Z, Liu Y, Lin C et al (2024c) Altered parietal operculum cortex 2 functional connectivity in benign paroxysmal positional vertigo patients with residual dizziness: a resting-state fMRI study. CNS Neurosci Ther 30(2):e14570. https://doi.org/10.1111/cns.14570
8. Chen Z, Xiao L, Liu Y et al (2024d) Altered hippocampal subfields functional connectivity in benign paroxysmal positional vertigo patients with residual dizziness: a resting-state fMRI study. CNS Neurosci Ther 30(12):e70175. https://doi.org/10.1111/cns.70175
9. Ciric R, Wolf DH, Power JD et al (2017) Benchmarking of participant-level confound regression strategies for the control of motion artifact in studies of functional connectivity. NeuroImage 154:174–187. https://doi.org/10.1016/j.neuroimage.2017.03.020
10. Esteban O, Markiewicz CJ, Blair RW et al (2019) fMRIPrep: a robust preprocessing pipeline for functional MRI. Nat Methods 16(1):111–116. https://doi.org/10.1038/s41592-018-0235-4
11. Ezaki T, Himeno Y, Watanabe T, Masuda N (2021) Modelling state-transition dynamics in resting-state brain signals by the hidden Markov and Gaussian mixture models. Eur J Neurosci 54(4):5404–5416. https://doi.org/10.1111/ejn.15386
12. Fu W, Bai Y, He F et al (2022) The association between precuneus function and residual dizziness in patients with benign paroxysmal positional vertigo. Front Neurol 13:828642. https://doi.org/10.3389/fneur.2022.828642
13. Lee JY, Lee IB, Kim MB (2021) Correlation between residual dizziness and modified clinical test of sensory integration and balance in patients with benign paroxysmal positional vertigo. Res Vestib Sci 20(3):93–100. https://doi.org/10.21790/rvs.2021.20.3.93
14. Lin C, Liu D, Liu Y et al (2023) Altered functional activity of the precuneus and superior temporal gyrus in patients with residual dizziness caused by benign paroxysmal positional vertigo. Front Neurosci 17:1221579. https://doi.org/10.3389/fnins.2023.1221579
15. Liu D, Lin C, Sun Y et al (2025) Altered cerebral gray matter volume and functional connectivity in patients with residual dizziness of benign paroxysmal positional vertigo. Clin Radiol 82:106780. https://doi.org/10.1016/j.crad.2024.106780
16. Long Z, Liu X, Niu Y et al (2023) Improved dynamic functional connectivity estimation with an alternating hidden Markov model. Cogn Neurodyn 17(5):1381–1398.

https://doi.org/10.1007/s11571-022-09874-3

17. Moretto M, Silvestri E, Zangrossi A, Corbetta M, Bertoldo A (2022) Unveiling whole-brain dynamics in normal aging through hidden Markov models. Hum Brain Mapp 43(3):1129–1144. https://doi.org/10.1002/hbm.25714
18. Parkes L, Fulcher B, Yücel M, Fornito A (2018) An evaluation of the efficacy, reliability, and sensitivity of motion correction strategies for resting-state functional MRI. NeuroImage 171:415–436. https://doi.org/10.1016/j.neuroimage.2017.12.073
19. Schaefer A, Kong R, Gordon EM et al (2018) Local-global parcellation of the human cerebral cortex from intrinsic functional connectivity MRI. Cereb Cortex 28(9):3095–3114. https://doi.org/10.1093/cercor/bhx179
20. Teh CSL, Mah MC, Rahmat K, Prepageran N (2022) Neuroimaging systematic review in persistent postural-perceptual dizziness: the elaborate alterations in the delicate network to remain balanced. Otol Neurotol 43(1):12–22. https://doi.org/10.1097/mao.0000000000003389
21. Vidaurre D, Masaracchia L, Larsen NY et al (2025) The Gaussian-linear hidden Markov model: a Python package. Imaging Neurosci 3:imaga00460. https://doi.org/10.1162/imag_a_00460
22. von Brevern M, Bertholon P, Brandt T et al (2015) Benign paroxysmal positional vertigo: diagnostic criteria. J Vestib Res 25(3–4):105–117. https://doi.org/10.3233/ves-150553
23. Wu J, Shu L, Zhou CY et al (2024) Brain functional alterations in patients with benign paroxysmal positional vertigo demonstrate the visual–vestibular interaction and integration. Brain Behav 14(10):e70053. https://doi.org/10.1002/brb3.70053
24. Xing Y, Si L, Wang Y, Zhang W, Ling X, Yang X (2024) Altered functional connectivity of the multisensory vestibular cortex in patients with chronic unilateral vestibulopathy. Brain Connect 14(4):252–259. https://doi.org/10.1089/brain.2023.0074
25. Yang K, Wang Y, Jia L et al (2026) Functional connectivity alterations in benign paroxysmal positional vertigo: insights from brain resting-state networks. AJNR Am J Neuroradiol 47(4):1031–1039. https://doi.org/10.3174/ajnr.a9048
26. Yeo BT, Krienen FM, Sepulcre J et al (2011) The organization of the human cerebral cortex estimated by intrinsic functional connectivity. J Neurophysiol 106(3):1125–1165. https://doi.org/10.1152/jn.00338.2011

Figures

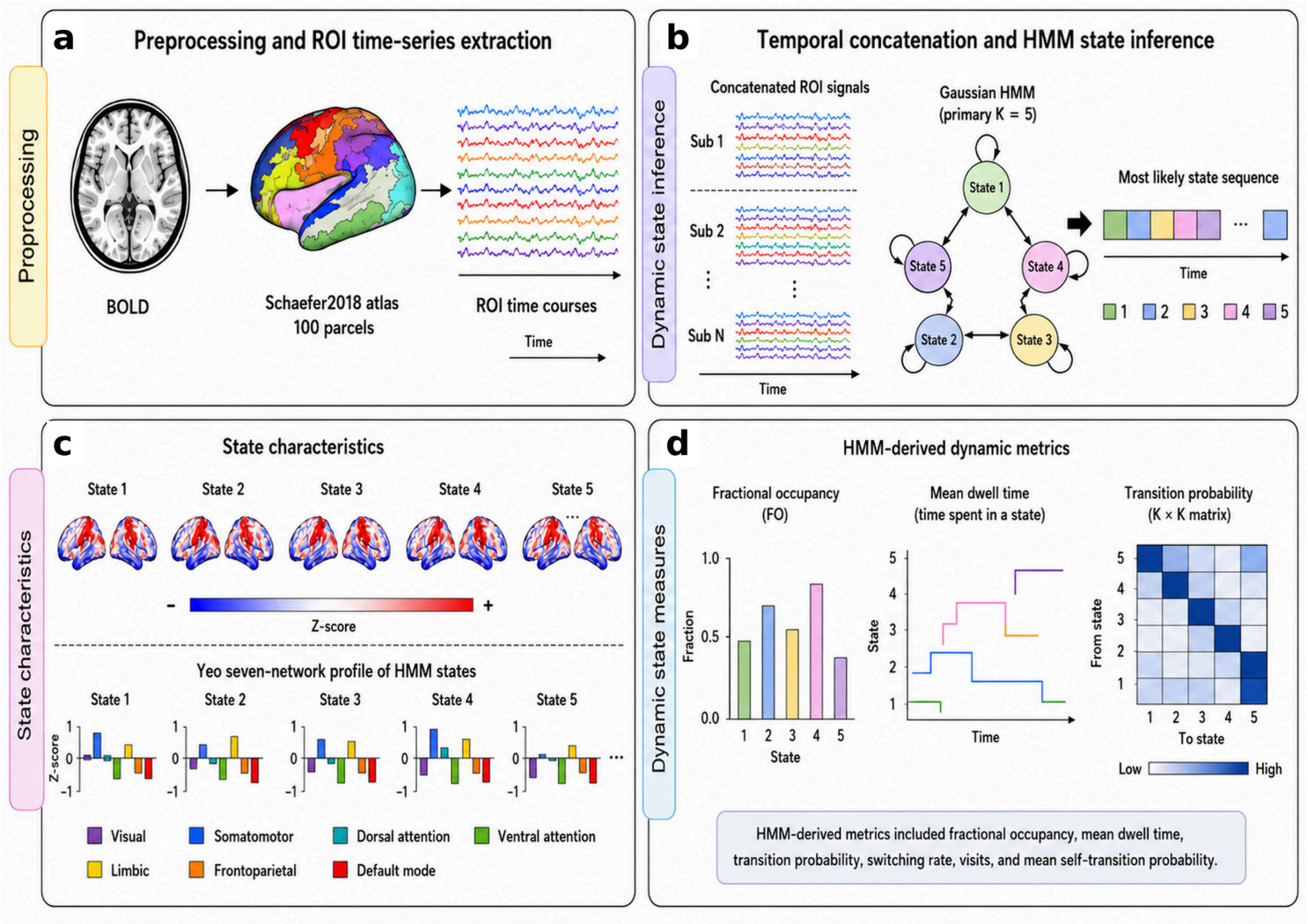


Figure 1

Study workflow and hidden Markov model analysis. (a) Resting-state fMRI data from 46 healthy controls and 70 patients with BPPV comprised 180 time points from 100 Schaefer 2018 cortical parcels. (b) Standardized parcel time series were concatenated with participant boundaries preserved. A prespecified five-state diagonal-covariance Gaussian HMM was fitted using 50 random initializations, and the highest-likelihood converged solution was used for Viterbi decoding. (c) The model yielded five cortical expression states and one decoded sequence per participant. (d) Derived measures included switching rate, mean dwell time, mean visits per state, mean empirical self-transition probability, fractional occupancy, and state-specific transition probabilities. BOLD, blood-oxygen-level-dependent; BPPV, benign paroxysmal positional vertigo; HMM, hidden Markov model; MRI, magnetic resonance imaging; ROI, region of interest

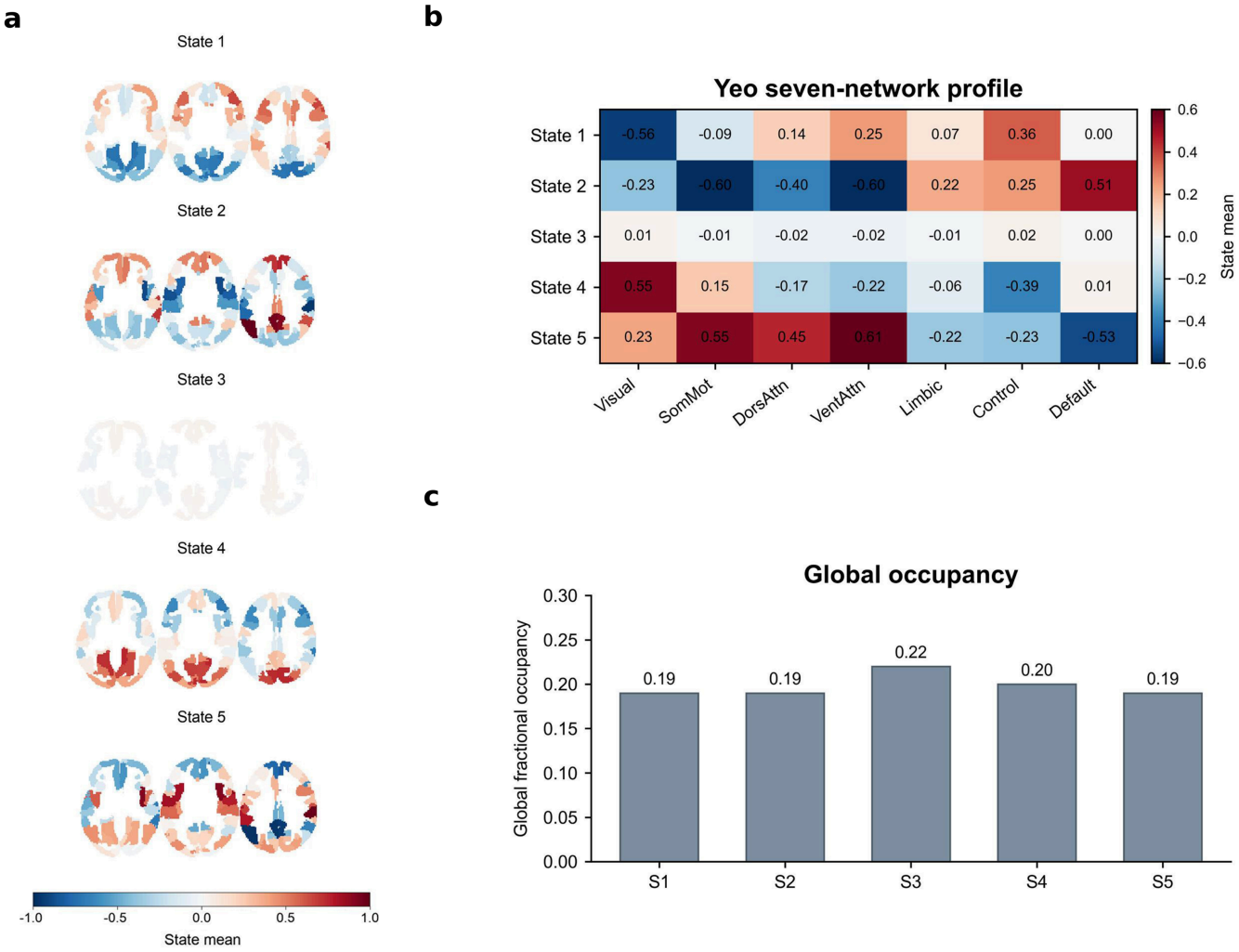


Figure 2

Cortical expression patterns in the primary five-state model. (a) State-specific mean expression across 100 Schaefer 2018 parcels. (b) Mean expression across the Yeo seven networks. (c) Fractional occupancy in the full sample. All maps use the same color scale; State 3 appears near the midpoint because its values are closer to zero. Values represent relative standardized expression, and state labels are model-specific. DAN, dorsal attention network; DMN, default mode network; FPN, frontoparietal network; LIM, limbic network; SMN, somatomotor network; VAN, ventral attention network; VIS, visual network

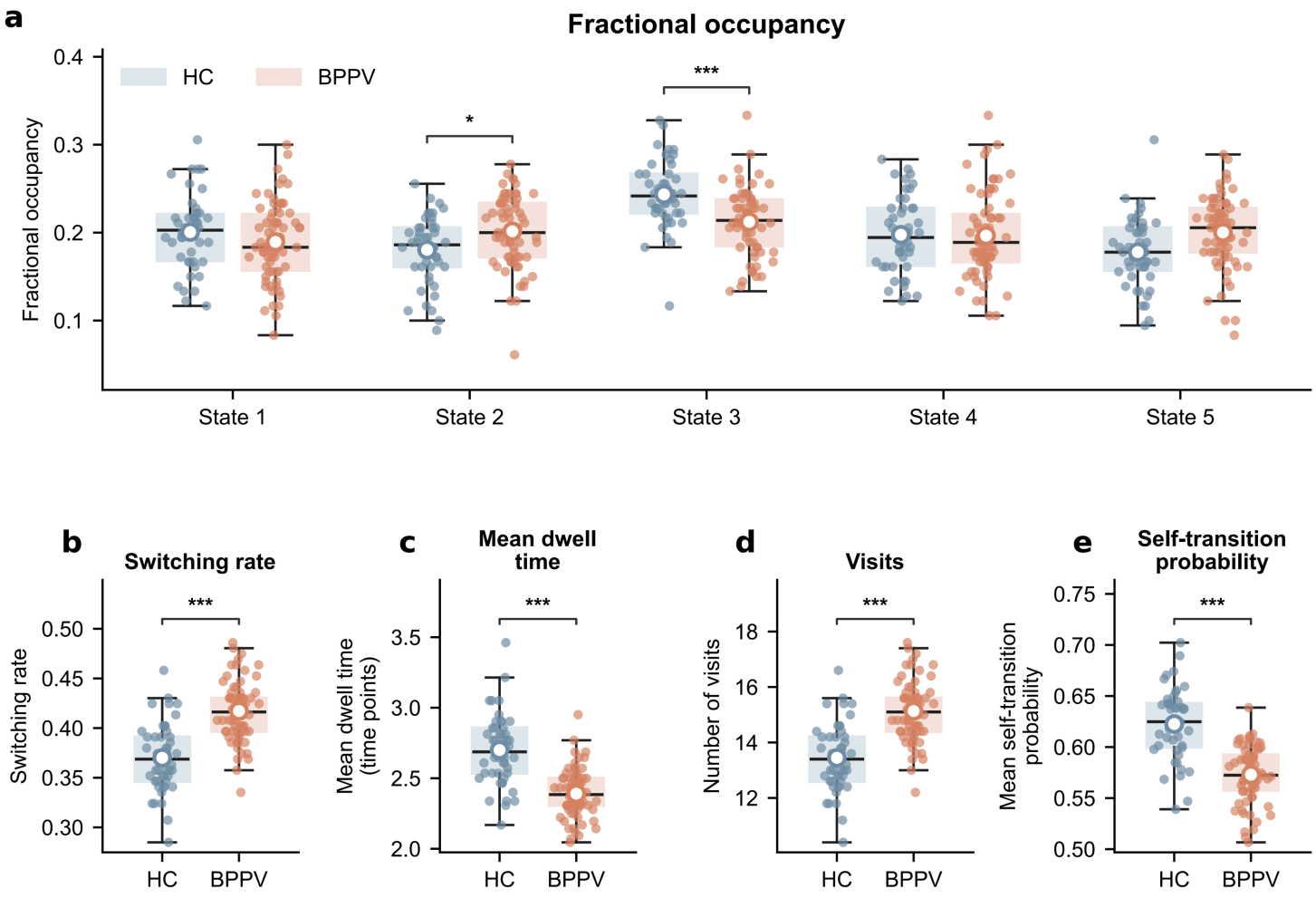


Figure 3

Global temporal measures and fractional occupancy in the primary five-state model. (a) Fractional occupancy. (b) Switching rate. (c) Mean dwell time. (d) Mean number of visits per state. (e) Mean empirical self-transition probability. Points represent individual participants. Boxes indicate the interquartile range, center lines indicate the median, and whiskers extend to the most extreme observations within 1.5 times the interquartile range. Group models included age, sex, years of education, and mean framewise displacement. BPPV, benign paroxysmal positional vertigo; HC, healthy control

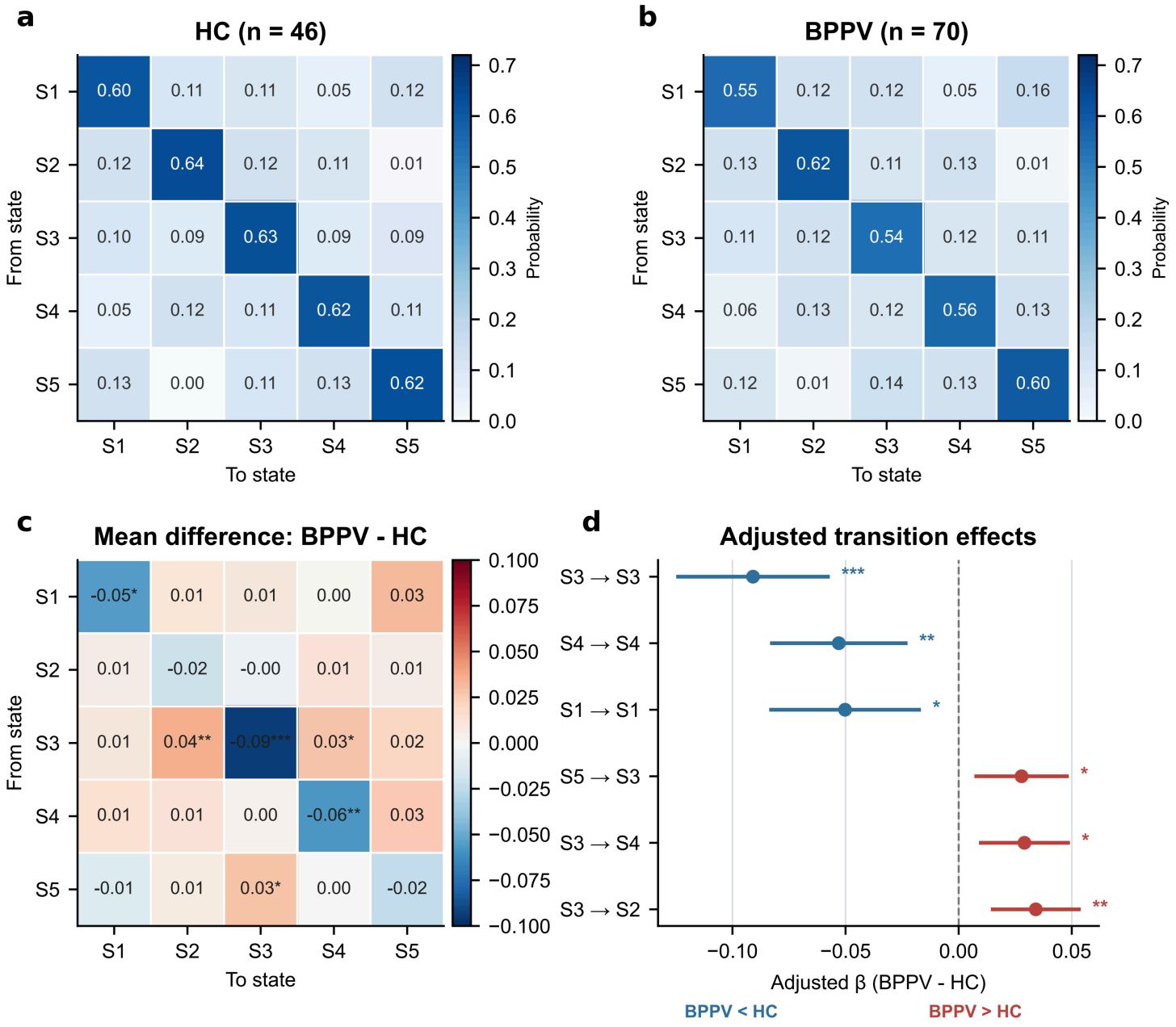


Figure 4

Secondary empirical transition differences in the primary five-state model. (a) Group-mean empirical transition matrix for healthy controls. (b) Group-mean empirical transition matrix for patients with BPPV. (c) Mean BPPV-minus-HC difference matrix. Rows indicate current states and columns indicate subsequent states. (d) Adjusted BPPV-minus-HC coefficients with 95% confidence intervals for the six transitions that survived false-discovery-rate correction across the 25 tests. Models included age, sex, years of education, and mean framewise displacement. The vertical line at zero indicates no adjusted group difference. BPPV, benign paroxysmal positional vertigo; HC, healthy control

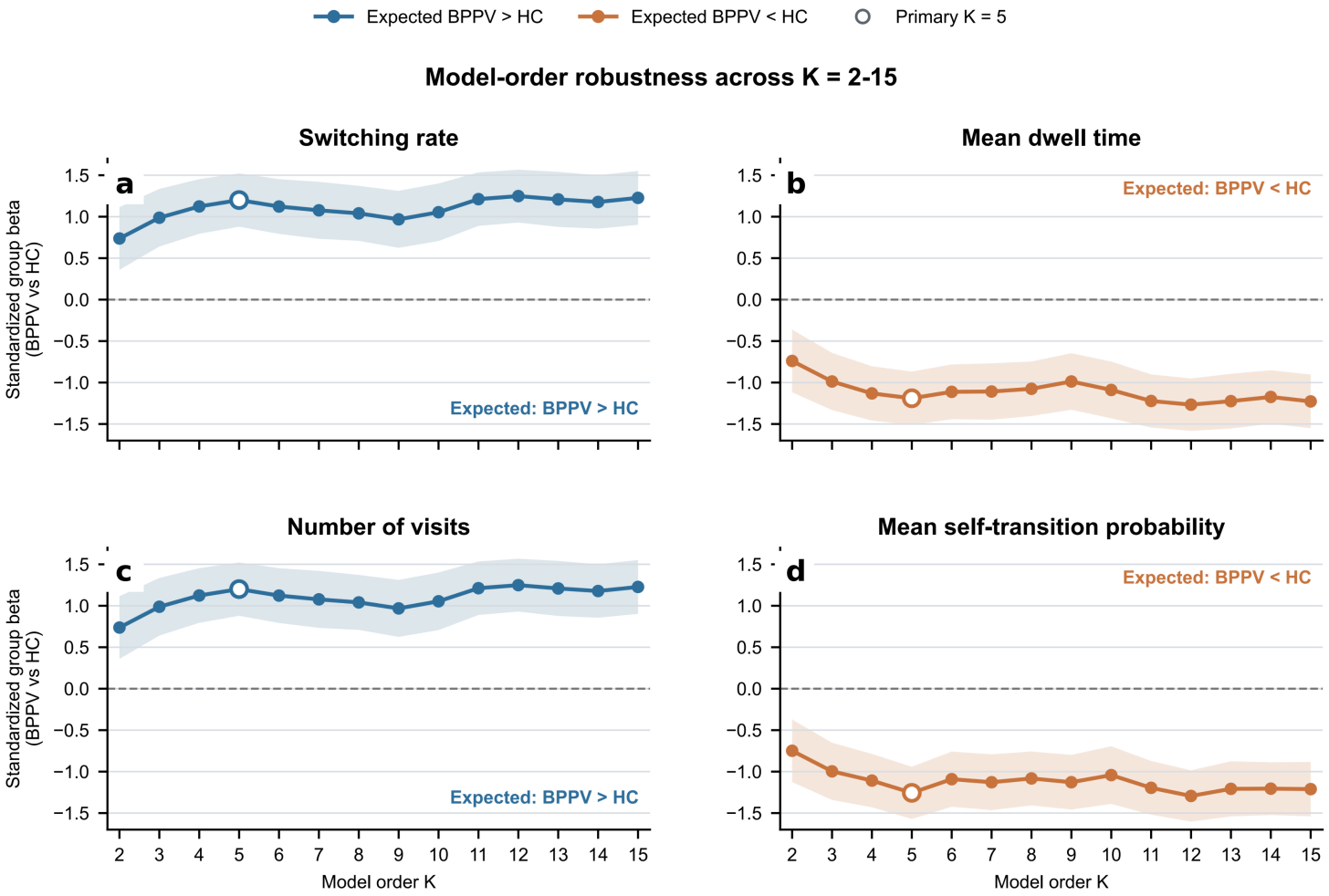


Figure 5

Model-order robustness of global temporal effects. Adjusted BPPV-minus-HC coefficients with 95% confidence intervals are shown in standard-deviation units across K = 2–15 for switching rate, mean dwell time, mean visits per state, and mean empirical self-transition probability. The primary K = 5 model is indicated by an open circle. States were fitted independently at each model order, and no state-to-state correspondence across model orders was assumed. BPPV, benign paroxysmal positional vertigo; HC, healthy control

Supplementary Files

This is a list of supplementary files associated with this preprint. Click to download.

- SupplementaryMaterial.pdf